Quantum critical point and spin fluctuations in lower-mantle ferropericlase

Igor S. Lyubutin[a], Viktor V. Struzhkin[b], A. A. Mironovich[c], Alexander G. Gavriliuk[a,b,c], Pavel G. Naumov[a], Jung-Fu Lin[d], Sergey G. Ovchinnikov[e,f], Stanislav Sinogeikin[g], Paul Chow[g], Yuming Xiao[g], and Russell J. Hemley[b,1]

[a]Institute of Crystallography, Russian Academy of Sciences, Moscow 119333, Russia; [b]Geophysical Laboratory, Carnegie Institution of Washington, Washington, DC 20015; [c]Institute for Nuclear Research, Russian Academy of Sciences, Troitsk, Moscow 142190, Russia; [d]Department of Geological Sciences, Jackson School of Geosciences, University of Texas at Austin, Austin, TX 78712; [e]L. V. Kirensky Institute of Physics, Siberian Branch of Russian Academy of Sciences, Krasnoyarsk 660036, Russia; [f]Siberian Federal University, Krasnoyarsk 660041, Russia; and [g]High Pressure Collaborative Access Team, Geophysical Laboratory, Carnegie Institution of Washington, Advanced Photon Source, Argonne National Laboratory, Argonne, IL 60439

Contributed by Russell J. Hemley, March 13, 2013 (sent for review July 13, 2012)

Ferropericlase [(Mg,Fe)O] is one of the most abundant minerals of the earth's lower mantle. The high-spin (HS) to low-spin (LS) transition in the Fe^{2+} ions may dramatically alter the physical and chemical properties of (Mg,Fe)O in the deep mantle. To understand the effects of compression on the ground electronic state of iron, electronic and magnetic states of Fe^{2+} in $(Mg_{0.75}Fe_{0.25})O$ have been investigated using transmission and synchrotron Mössbauer spectroscopy at high pressures and low temperatures (down to 5 K). Our results show that the ground electronic state of Fe^{2+} at the critical pressure P_c of the spin transition close to $T = 0$ is governed by a quantum critical point ($T = 0$, $P = P_c$) at which the energy required for the fluctuation between HS and LS states is zero. Analysis of the data gives P_c = 55 GPa. Thermal excitation within the HS or LS states ($T > 0$ K) is expected to strongly influence the magnetic as well as physical properties of ferropericlase. Multielectron theoretical calculations show that the existence of the quantum critical point at temperatures approaching zero affects not only physical properties of ferropericlase at low temperatures but also its properties at *P-T* of the earth's lower mantle.

diamond anvil cell | synchrotron radiation | Mott insulator | spin crossover

Ferropericlase [$(Mg_{1-x}Fe_x)O$ with x = 0.15–0.20] in the face-centered cubic rock-salt structure is believed to be the second most abundant mineral phase in the earth's lower mantle. It has ~16% abundance by volume, together with silicate perovskite [$(Mg_{1-x}Fe_x)SiO_3$], which has a 79% abundance (1–6). Great interest recently has been focused on the pressure-induced electronic transition in (Mg,Fe)O, in which the Fe^{2+} ions transform from the high-spin (HS) state [total spin momentum (S) = 2] to the low-spin (LS) state (S = 0) (7–14). A series of observed physical and chemical properties of (Mg,Fe)O have been altered dramatically by the spin transition in the relevant range of pressure–temperature (*P-T*) conditions of the deep earth's mantle, including thermal (15, 16) and electrical (17) conductivity, density (18, 19), incompressibility (18), and sound velocity (20). Most previous investigations on the spin transition of iron in ferropericlase were performed at either room temperature or high temperatures. At pressures near the spin cross-over, the Fe ions may exist in a mixed condition, with HS and LS states coexisting as the result of thermal fluctuations. This mixed state results in a wide cross-over with a smooth, continuous transition from the HS to the LS state with a pressure interval (ΔP) of ~20 GPa (9, 14). Studies on the electronic and magnetic states at low temperatures may provide crucial information on the ground state of the Fe ions in ferropericlase at high pressures (21).

We have investigated electronic and magnetic properties of Fe^{2+} in two representative compositions of ferropericlase $(Mg_{1-x}Fe_x)O$ (x = 0.25 and 0.2) at high pressures and low temperatures using transmission Mössbauer spectroscopy (TMS) and synchrotron Mössbauer spectroscopy (also called nuclear forward scattering, NFS) in diamond anvil cells (DACs) up to 90 GPa. Hyperfine parameters of iron ions derived from the Mössbauer spectra are used to construct the magnetic phase diagram. We find quantum critical point in the phase diagram at 55 GPa and low temperatures where the excitation energy of the HS or/and LS states is zero. Based on multielectron theoretical calculations (22, 23), we predict unique magnetic properties in (Mg,Fe)O to occur at *P-T* conditions relevant to the earth's lower mantle.

Results and Discussion

Ambient-Pressure, Low-Temperature Mössbauer Spectra. Low-temperature TMS spectra at ambient pressure are shown in Fig. 1*A* for $(Mg_{0.75}Fe_{0.25})O$ and in Fig. 1*B* for $(Mg_{0.8}Fe_{0.2})O$. At 5 K, the spectral lines are split as a result of the magnetic hyperfine interaction, indicating the magnetic ordering of the Fe^{2+} ions. Magnetic splitting decreases gradually with increasing temperature. Above 40 K, the spectral features are dominated by a doublet typical of the paramagnetic state (14). In the magnetic region, the spectral lines are very broad and asymmetric. The line broadening may be explained by the presence of many nonequivalently distributed Fe^{2+} sites through nearest-neighbor interactions (14). On the other hand, the asymmetric spectral shape may be explained by the higher electric quadrupole interaction, which becomes comparable with the magnetic hyperfine interaction at temperatures near the Néel temperature (T_N) (24).

Using standard procedures for analyses of the Mössbauer spectra (25), we plotted the distribution functions for the hyperfine parameters and estimated the averaged value of the magnetic hyperfine field at the iron nuclei $\langle H_{hf} \rangle$. The temperature-dependent $\langle H_{hf} \rangle$ values are shown in Fig. 1 *C* and *D* for $(Mg_{0.75}Fe_{0.25})O$ and $(Mg_{0.8}Fe_{0.2})O$, respectively. Based on this behavior, we also have evaluated the Néel temperatures T_N as ~37 K and ~27 K for $(Mg_{0.75}Fe_{0.25})O$ and $(Mg_{0.8}Fe_{0.2})O$, respectively. The latter T_N value for $(Mg_{0.8}Fe_{0.2})O$ is close to the 25 K value given by Speziale et al. (21). It is known that pure wüstite (FeO), an end member of the $(Mg_{1-x}Fe_x)O$ series, is an antiferromagnet with the T_N = 198 K (26), and its crystal structure changes from cubic to rhombohedral upon the magnetic transition at high pressures (6, 26). The magnetic ordering is governed mainly by strong superexchange antiferromagnetic interactions in Fe-O-Fe with a bond angle of about 180°. Similarly, the magnetic properties of the $(Mg_{1-x}Fe_x)O$ solid solution depend on the iron concentration x and also may be determined from the Fe-O-Fe superexchange interactions. In a random mixture of Mg/Fe ions, long-range magnetic ordering may

Author contributions: I.S.L., V.V.S., and R.J.H. designed research; A.A.M., A.G.G., J.-F.L., S.S., P.C., and Y.X. performed research; S.G.O. developed the theoretical model; I.S.L., V.V.S., A.G.G., P.G.N., and S.G.O. analyzed data; and I.S.L., V.V.S., A.A.M., A.G.G., J.-F.L., S.G.O., and R.J.H. wrote the paper.

The authors declare no conflict of interest.

[1]To whom correspondence should be addressed. E-mail: hemley@gl.ciw.edu.

This article contains supporting information online at www.pnas.org/lookup/suppl/doi:10.1073/pnas.1304827110/-/DCSupplemental.

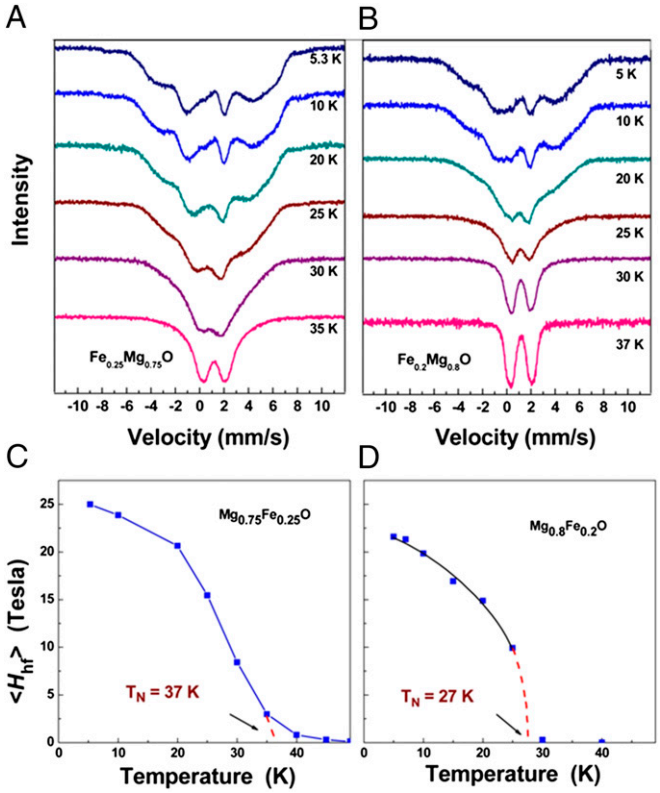

Fig. 1. Representative low-temperature transmission ^{57}Fe-Mössbauer spectra at ambient pressure. (*A*) $(Mg_{0.75}Fe_{0.25})O$; (*B*) $(Mg_{0.8}Fe_{0.2})O$. Temperature-dependent average values of magnetic hyperfine field $<H_{hf}>$ at iron nuclei obtained from the spectra of $(Mg_{0.75}Fe_{0.25})O$ (*C*) and $(Mg_{0.8}Fe_{0.2})O$ (*D*). Solid and dashed lines are guides to the eye.

appear at iron concentrations above the critical value x_c (the percolation threshold). For a 3D *fcc* lattice, the critical value is close to $x_c \sim 0.16$ (27). Thus, both compounds studied here have iron concentrations above the percolation threshold and may exhibit a long-range magnetic order below T_N.

Based on the analyses of the ambient-pressure Mössbauer spectra, we also have examined the behavior of the quadrupole splitting ε, the isomer shift δ, and the area under the resonance lines *I* in the paramagnetic state at temperatures between T_N and 300 K. As shown in Fig. 2, the average value of the quadrupole splitting in $(Mg_{0.75}Fe_{0.25})O$ and $(Mg_{0.8}Fe_{0.2})O$ decreases continuously from about 1.90 to 0.75 mm/s, whereas the isomer shift decreases in accordance with the relativistic second-order Doppler effect (the temperature shift) (24). Considering the area *I* under the resonance lines, we fitted the experimentally derived *I* values using the Debye approximation (28) and evaluated values for the "Mössbauer" Debye temperatures (θ_D). For the local Fe^{2+} sites in $(Mg_{0.75}Fe_{0.25})O$ and $(Mg_{0.8}Fe_{0.2})O$, the Debye temperatures are 290 (±10) K and 450 (±10) K, respectively.

Synchrotron Mössbauer Spectra at High Pressures and Low Temperatures. The NFS spectra of $(Mg_{0.75}Fe_{0.25})O$ were recorded at high pressures up to 60 GPa and at temperatures between 8 K and 300 K (Fig. 3 *A* and *B*). Contrary to the TMS technique, in which the resonance signal is recorded as a function of energy of the Mössbauer gamma-quanta, the NFS signal is recorded as a function of time. The time spectra represent damping decays of the nuclear excitation that is modulated in time by quantum and dynamic beats (see details in refs. 29 and 30). At lower temperatures of 12 K and 15 K, the high-frequency quantum beats of the magnetic signature are present in the spectra (Fig. 3*A*), indicating the occurrence of magnetic ordering of the iron ions. Above 50 K, only low-frequency quantum beats can be seen in the NFS spectra, revealing the paramagnetic state (Fig. 3*A*). Analyses of the shapes of the quantum beats show that the samples transform from a low-frequency paramagnetic state to a high-frequency magnetic state at pressures below 55 GPa during temperature cooling cycles (Fig. 3*A*). The low-frequency quantum beats appear to be a result of the electric quadrupole interaction of the ^{57}Fe nuclei with the electric field gradient at the local iron sites. Disappearance of the magnetic quantum beats at $P < 55$ GPa may be considered the transition from the magnetically ordered state to the paramagnetic state (both are in the HS state). Based on the analyses of the NFS spectra, we have derived the Néel temperatures of the samples at pressures below 55 GPa (all details of the spectra analyses are given in *SI Materials and Methods*). It should be noted that the magnetic behavior of ferropericlase $(Mg_{0.75}Fe_{0.25})O$ may be rather complicated at temperatures below the T_N because of the existence of many nonequivalent iron sites (14) and the percolation effects in the magnetically diluted system.

At pressures above 55 GPa, the low-frequency quantum beats of the electric quadrupole signature disappear at T < 50 K and the NFS spectra of the nuclei decay appear as straight lines (Fig. 3*B*). This spectral shape corresponds to a singlet in the TMS spectra with a zero quadrupole splitting (14), showing the occurrence of the LS state of Fe^{2+}. Above 90 K, the low-frequency quantum beats appear in the spectra, showing the presence of the paramagnetic HS state with increased abundance with increasing temperatures (Fig. 3*B*). Near the critical pressure of 55 GPa, we have observed the coexistence and fluctuations of the HS and LS Fe^{2+} irons with relative abundance changing dramatically with temperature. That is, we have observed the thermal activation effect on the iron spin states at extreme conditions.

The HS-LS coexistence at finite temperatures may be understood in terms of the thermal fluctuations through a spin gap. The spin-gap energy ε_S is given by the excitation energy between the HS term $^5T_2$ and the LS term $^1A_1$

$$\varepsilon_S = E_{HS}(d^6,\ ^5T_2) - E_{LS}(d^6,\ ^1A_1). \qquad [1]$$

Near the critical pressure P_c, the ε_S value is proportional to $(P - P_c)$. As is shown below, at $P > P_c$ the thermally activated

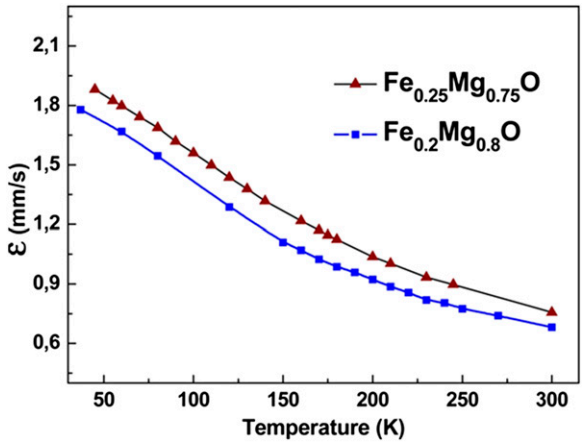

Fig. 2. Temperature-dependent quadrupole splitting parameter (ε) obtained from the ^{57}Fe-Mössbauer spectra in the paramagnetic region of $(Mg_{0.75}Fe_{0.25})O$ (brown) and $(Mg_{0.8}Fe_{0.2})O$ (blue) ($\varepsilon = e^2qQ/2$, where *Q* is the nuclear quadrupole moment and $eq = V_{zz} = \partial^2 V/\partial z^2$ is the electric field gradient). Solid lines are guides to the eye.

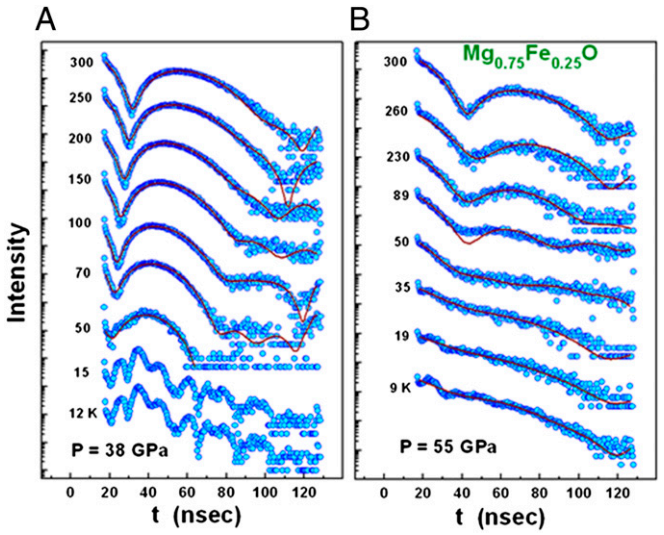

Fig. 3. Representative low-temperature synchrotron Mössbauer spectra of $(Mg_{0.75}Fe_{0.25})O$ at 38 GPa (*A*) and 55 GPa (*B*). High-frequency quantum beats indicate a magnetic ordering of Fe^{2+} ions in the HS state, whereas the low-frequency quantum beats indicate the paramagnetic state of Fe^{2+} ions in the HS state. Absence of the quantum beats indicates the occurrence of the diamagnetic state of the LS Fe^{2+} ions. Solid lines are calculated data.

magnetic moment may appear (from the HS Fe^{2+} ions) with a maximum in temperature-dependent magnetization at $T \sim \varepsilon_S$.

Quantum Critical Point in the $(Mg_{0.75}Fe_{0.25})O$ Phase Diagram. The magnetic phase diagram of $(Mg_{0.75}Fe_{0.25})O$ shown in Fig. 4 is constructed using analyzed Mössbauer data at high pressures and low temperatures. The diagram shows regions of the HS paramagnetic and antiferromagnetic phases up to 55 GPa, and the LS diamagnetic phase above 55 GPa. The pressure-dependent Néel temperatures (the dashed blue line in Fig. 4) up to 55 GPa separate the magnetically ordered and paramagnetic HS states of $(Mg_{0.75}Fe_{0.25})O$. The T_N increases with increasing pressure and reaches a maximum at about 55 K and 30 GPa, but drops dramatically as the critical point of the HS-LS cross-over is approached. At the absolute zero temperature and the critical pressure of 55 (±3) GPa, a quantum critical point appears in the magnetic phase diagram.

The physical meaning of the quantum critical point at $T = 0$ and $P = P_c$ is clarified below. At $T = 0$ and $P < P_c$, the ground state of the Fe^{2+} ion in the HS state has the wave function $\Psi(HS)$. At each pressure in the $P < P_c$ range, the LS state is separated from the HS state by the energy $|\varepsilon_S|$ and can be populated by thermal excitations only. Above P_c at $T = 0$, the ground state of Fe^{2+} is the LS state, which has the wave function $\Psi(LS)$. The HS state is separated from the LS state by the energy $|\varepsilon_S|$ and also can be populated only by thermal excitation. In the quantum critical point ($T = 0$, $P = P_c$), the energies of the HS and LS states are equal. The wave function for the Fe^{2+} ion is given by a mixture of these wave functions, $\Psi(d^6) = c_1 * \Psi(HS) + c_2 * \Psi(LS)$, where c_1 and c_2 are numerical coefficients. The quantum spin fluctuations between HS and LS states (HS → LS, LS → HS) do not require any energy at the critical point because the HS and LS states have the same energy. We should emphasize here that these are fluctuations of the spin value, in contrast to the conventional fluctuations of the spin direction in the magnetic state. That is, the quantum spin fluctuations dramatically suppress the magnetic order at the critical point.

It has been shown in recent years that quantum critical point phenomena appear in many quantum systems in which the thermodynamic order parameter (here the sublattice magnetization in the antiferromagnetic HS state) disappears at $T = 0$ under some external influences (such as the high-pressure variable investigated here) (31). The quantum phase transition has a Berry phase-like topological order parameter (31, 32), and the quantum fluctuations in the critical point are the electronic HS-LS fluctuations between two degenerate HS and LS terms.

The red shaded area in Fig. 4 shows the region of the coexisting HS and LS states. The coexistence of the different spin states at finite temperatures has been observed experimentally in several Fe^{3+}-containing oxides (33–35) and has been explained as the consequence of the thermal fluctuation effects between the electronic HS (S = 5/2) and LS (S = 1/2) Fe^{3+} states (33). Additionally, the coexistence of the HS and LS Fe^{2+} has been found in $(Mg_{0.75}Fe_{0.25})O$ at temperatures between 300 K and 2,000 K using X-ray emission spectroscopy in a laser-heated DAC (36). As was shown previously (35), the width of the coexisting region depends strongly on temperature, and decreases dramatically as the temperature approaches zero because of the suppression of the thermal fluctuations.

Our high-pressure TMS and NFS measurements of $(Mg_{0.75}Fe_{0.25})O$ performed under hydrostatic conditions using helium as the pressure medium have manifested the pressure interval (53–68 GPa) for the coexistence of the HS Fe^{2+} and LS Fe^{2+} states at room temperature. Detailed evaluations concerning the width of the coexisting HS and LS Fe^{2+} states in our study are given in *SI Materials and Methods*.

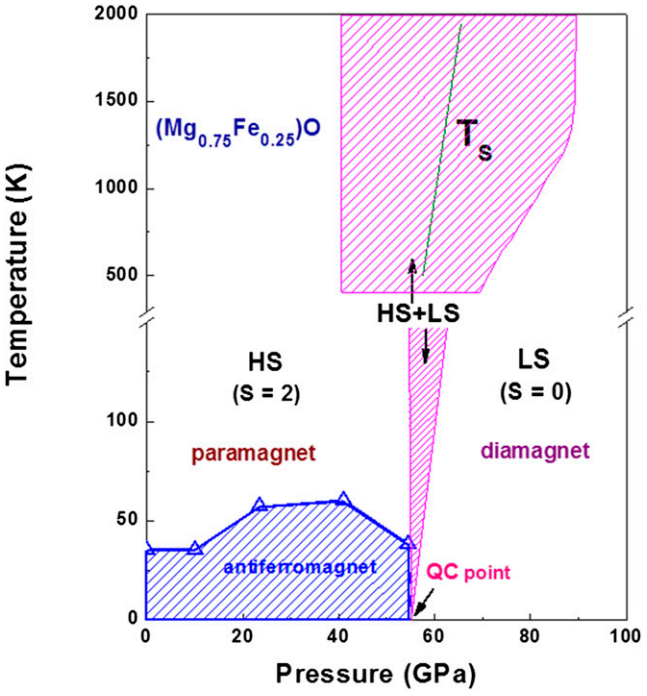

Fig. 4. Magnetic phase diagram of ferropericlase $(Mg_{0.75}Fe_{0.25})O$ at high pressures and low temperatures. The solid blue line separates the regions of the HS paramagnetic and antiferromagnetic phases between 0 GPa and 50 GPa. Above 55 GPa, the diagram shows the LS diamagnetic phase, which appears as a result of the HS → LS cross-over. A quantum critical point appears in the diagram at $T = 0$ and $P = P_c$ that may be explained in terms of the geometric phase of the topological origin that is considered an order parameter in the spin cross-over phenomena (33). In the shaded (red) area, the HS and LS states coexist because of the thermal fluctuations between the electronic HS and LS states. In the upper part of this area (shaded red), the region of the coexisting HS and LS states is extended to high temperatures relevant to the lower-mantle conditions (calculated from ref. 31 experimental data). The dashed line in this area indicates the position of maximum of the magnetic susceptibility χ of ferropericlase.

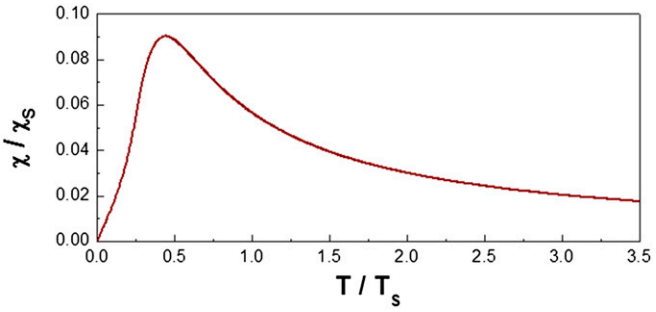

Fig. 5. Expected temperature dependence of the magnetic susceptibility above the critical pressure P_c of the HS-LS cross-over at the earth's lower-mantle conditions. T_S is the spin-gap value (in the temperature scale) that is proportional to $(P - P_c)$. At $T << T_S$, the admixture of excited HS term into the nonmagnetic LS state results in an increase of magnetization and susceptibility. At $T >> T_S$, the χ value, generated by the excited HS state, decreases as a result of the standard Curie law. These two opposite regimes result in a maximum of χ at $T \sim T_S$. $\chi/\chi_s = n_{HS}T_s/T$, with $\chi_s = N_A\, S(S+1)\, \mu_B{}^2 g_{HS}/k_B T_s$, and N_A is the Avogardo number, μ_B is the Bohr magneton, g_{HS} and n_{HS} are the HS degeneracy and fraction given below by Eq. **6**.

Magnetic Properties of Ferropericlase in the Earth's Lower Mantle. Because the spin transition is of great interest in earth science, here we have used theoretical calculations to extend the experimental results to high *P-T* relevant to the lower mantle. The magnetic properties of ferropericlase have been analyzed above the critical pressure P_c using the multielectron generalized tight-binding (GTB) approach (22, 23). In the d^6 state of Fe^{2+}, the critical pressure is determined by the cross-over of the HS ($^5T_2$) and LS ($^1A_1$) terms with the energies (23)

$$E_{HS}\left(d^6,\ {}^5T_2\right) = 6\varepsilon_d + 15A - 21B - 4Dq, \qquad [2]$$

$$E_{LS}\left(d^6,\ {}^1A_1\right) = 6\varepsilon_d + 15A - 16B + 8C - 24Dq, \qquad [3]$$

where ε_d is a single *d*-electron atomic energy; *A*, *B*, and *C* are the Racah parameters; and $10Dq$ is the crystal field-splitting energy in the cubic system. With increasing pressure, the crystal field-splitting energy increases as $10Dq(P) = 10Dq + \alpha P$. All other parameters are intraatomic and thus are pressure independent. The critical pressure P_c thus may be represented as $(2.5B + 4C - 10Dq)/\alpha$.

In the present calculations, we use the Racah parameters $A = 2$ eV, $B = 0.084$ eV, and $C = 0.39$ eV, obtained for Fe^{3+} ions in $FeBO_3$ (23), because the difference in the parameter values for Fe^{2+} and Fe^{3+} has been shown to be negligible (23). The crystal field-splitting energy is material dependent, and $10Dq = 1.34$ eV is used for ferropericlase at ambient pressure (13). Using these parameters and the experimentally determined $P_c = 55$ GPa, we find $\alpha = 0.0078$ eV/GPa.

At pressures above the critical point, one then can estimate the value of the spin gap ε_S using the equation

$$\begin{aligned}\varepsilon_S &= E_{HS}\left(d^6,\ {}^5T_2\right) - E_{LS}\left(d^6,\ {}^1A_1\right) + 2\alpha P \\ &= 2(10Dq - 2.5B - 4C + \alpha P) = 2\alpha(P - P_c).\end{aligned} \qquad [4]$$

This gap sharply increases with pressure, for instance, $\varepsilon_S = 0.156$ eV at $(P - P_c) = 10$ GPa. At a given pressure above P_c, it permits determination of the abundance of the thermally excited HS Fe^{2+} state; however, this abundance also is temperature dependent. At low temperatures, all Fe^{2+} ions are in the LS state at $P > P_c$ and magnetization is zero. At high temperatures, the magnetic moment may appear from the thermoactivated HS Fe^{2+} ions.

Similar electronic structures and magnetic properties have been found in $LaCoO_3$ at ambient pressure. Indeed, the Co^{3+} (d^6) ion has the LS ($^1A_1$) ground state with a small spin gap $\varepsilon_S \sim 150$ K (39, 40). Local density approximation (LDA)+GTB calculations of $LaCoO_3$ (41) have confirmed the known temperature-dependent magnetic susceptibility χ with the maximum at $T_S = \varepsilon_S/k_B$ (k_B is the Boltzmann constant). The same behavior in the temperature-dependent susceptibility also is expected for the LS ferropericlase (Fig. 5). The $\chi(T)$ dependence is determined by the competition between two major factors: (*i*) At low temperatures ($T << T_S$), the small admixture of the excited HS term into the nonmagnetic LS ($S = 0$) state results in an increase in the magnetization and susceptibility $\chi(T)$. (*ii*) At high temperatures ($T >> T_S$), the $\chi(T)$ value, generated by the excited HS state, decreases as a result of the standard Curie law. These two opposite regimes coexist at $T \sim T_S$, resulting in a $\chi(T)$ maximum (Fig. 5). The corresponding temperature T_S is given by $k_B T_S = 2\alpha(P - P_c)$, and its calculated value is $T_S = 1{,}812$ K and $3{,}624$ K at $(P - P_c) = 10$ and 20 GPa, respectively. The dashed line in the red shaded area of the phase diagram in Fig. 4 indicates the *P-T* line where the χ maximum is expected at the lower-mantle conditions.

Further considerations of the high-temperature spin cross-overs of Fe^{2+} in ferropericlase (Fig. 6) have revealed that the difference in the spin and orbital degeneracy of the HS and LS terms results in an asymmetry of the phase diagram as the fraction of HS and LS states varies with high *P-T*. The fraction of the HS state is given by

$$\begin{aligned}n_{HS}(P,T) &= \frac{g_{HS}\exp(-E_{HS}/kT)}{g_{HS}\exp(-E_{HS}/kT) + g_{LS}\exp(-E_{LS}/kT)} \\ &= \frac{1}{1 + \frac{g_{LS}}{g_{HS}}\exp\left(\frac{E_{HS} - E_{LS}}{kT}\right)}.\end{aligned} \qquad [5]$$

At $g_{HS} = g_{LS}$, the HS and LS (P,T) distribution would be symmetrical relative to the $P_c(T)$ line. However, for the HS-d^6 state, the spin and orbital values are $S = 2$ and $L = 1$, respectively, leading to $g_{HS} = (2S+1)(2L+1) = 15$, whereas for the LS-$d^6$ state these values are $S = 0$, $L = 0$, and $g_{LS} = 1$ (Fig. 6*A*). The sharp transformation of the HS state into the LS state at zero temperature reflects the effect of the quantum phase transition. At $T \neq 0$, the line in the *P-T* plane with a fixed fraction n_{HS} is given by the following equation:

$$P(n_{HS}) = P_c + kT/(2\partial\varepsilon_S/\partial P) \times \ln(n_{LS}g_{HS}/n_{HS}g_{LS}), \qquad [6]$$

where $P(n_{HS})$ is the pressure, the relative fraction of HS Fe^{2+} ions is n_{HS}, and the fraction of the LS Fe^{2+} ions is $n_{LS} = (1 - n_{HS})$. This

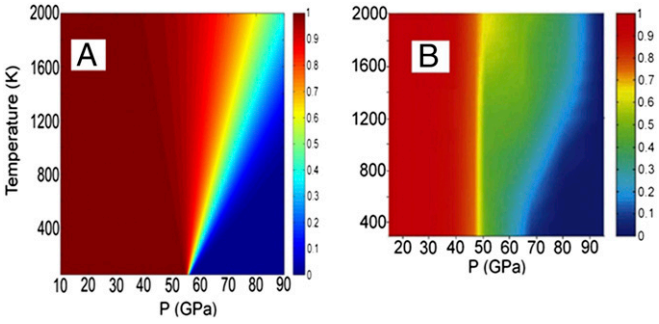

Fig. 6. Phase diagram of spin cross-over of Fe^{2+} in $(Mg_{0.75}Fe_{0.25})O$ calculated from Eq. **6** (*A*) and measured in ref. 31 by X-ray emission spectroscopy with laser heating (*B*). Colors in the vertical columns on the right represent fractions of the high-spin iron n_{HS}.

equation describes each *P-T* point in the diagram and relates to particular fractions of the HS and LS states. The *P-T* relationship is shown to be linear for each given n_{HS} value, thus a set of lines with different n_{HS} begins in the quantum critical point (Fig. 6*A*).

The spin-transition diagram of ferropericlase $(Mg_{0.83}Fe_{0.17})O$ at high *P-T* has been calculated (42) using a mean-field theoretical approach similar to ours. These authors discussed the high-temperature region with the minimal temperature at 300 K and found a gradual change in the spin state of iron with increasing temperature. At these conditions, their phase diagram is in qualitative agreement with our results. However, Sturhahn et al. (42) did not pay particular attention to the properties of the spin cross-over at zero temperature, and no indication of the quantum critical point was given.

At temperatures of 2,000 K, conditions are relevant to the earth's lower mantle (Fig. 6*A*). However, at $T = 0$ K, the quantum spin fluctuations are strongest at pressures near $P = 55$ GPa, whereas the thermal spin fluctuations are stronger near $P = 90$ GPa at 2,000 K. For comparison, we plotted the experimental data obtained for the ferropericlase by X-ray emission spectroscopy with laser heating (36) in Fig. 6*B*. General agreement of the calculated and measured diagrams is shown clearly in the diagram. Deviations in these studies may be explained by the contribution of the high-energy excitation terms of the Fe^{2+} ion, including the intermediate spin $S = 1$ state with the excitation energy ~1 eV. Other possible sources of the quantitative disagreement with our experimental data are the neglected electron–lattice interaction and lattice effects, which might be important because of a 10% difference in the ionic radii of HS/LS states. Previously, similar distributions of the HS fraction in (P,T) plane have been obtained by mean-field (42) and LDA+U (43) calculations. For a better description of the ferropericlase properties under high pressure, vibrational effects and electron–lattice interactions also should be taken into account (44–46), although we have limited our considerations to the main effect of the spin cross-over through the energy competition between the HS and LS states.

Conclusions

The present study reveals the existence of the quantum critical point at $T = 0$ and $P_c = 55$ GPa in ferropericlase $(Mg_{0.75}Fe_{0.25})O$. The main novelty of the approach may be summarized as (*i*) the multielectron calculations of the Fe^{2+} ion energies taking into account strong electron correlations; (*ii*) the unification of the continuous high-temperature spin cross-over with the sharp quantum phase transition at zero temperature; and (*iii*) calculations of the magnetic susceptibility as a function of *P* and *T*. High excitation energy ~1 eV (~10,000 K) necessary for activation of the nearest exited level of Fe^{2+} with the intermediate spin state ($S = 1$) in the system permits the extrapolation of our low-temperature phase diagram to high temperatures T ~2,000 K relevant to *P-T* conditions in the earth's low mantle. Our results (Fig. 6*A*) show that the spin transition in the earth's lower mantle is a continuous cross-over. Considering the *P-T* conditions along a geotherm (47), the smooth transformation of the spin state takes place at pressures between 55 GPa and 90 GPa, corresponding to the mid-lower mantle conditions over a depth of ~1,500–1,900 km. Because lower-mantle ferropericlase is expected to be subjected to pressures up to 136 GPa and temperatures as high as ~2,800 K, the extreme pressure is expected to increase the spin gap and thus to increase the T_S value.

The melting point of pure MgO is ~3,000–3,400 K at ambient pressure (48, 49) and increases to about 4,000 K (48) or even to 6,000 K (49, 50) with increasing pressure to 50 GPa. At such extreme temperatures, it is rather difficult for us to address the behavior of ferropericlase at temperatures above its melting point using our data here. At a given depth of the lower mantle, as long as the geotherm is below the melting temperature of ferropericlase, our conclusions here should be valid. Our model predicts that ferropericlase may exist in a paramagnetic state, even at the middle layer of the lower mantle at depths up to 1,900 km. It is conceivable that the occurrence of the paramagnetic ferropericlase with distinct physical and chemical properties may deeply influence our understanding of the geophysics, geochemistry, and geodynamics of the planet's interior.

Materials and Methods

Polycrystalline $(Mg_{0.75}Fe_{0.25})O$ and $(Mg_{0.8}Fe_{0.2})O$ samples with 95% (wt/wt) or 20% (wt/wt) ^{57}Fe enrichment, respectively, were synthesized by the ceramic method (7). X-ray diffraction patterns showed that the samples had the rock-salt structure, and neither magnetite (Fe_3O_4, in the spinel structure) nor hematite (α-Fe_2O_3, in corundum structure) was detected in the X-ray diffraction patterns. The ^{57}Fe-Mössbauer spectral analyses revealed the synthesized $(Mg_{0.8}Fe_{0.2})O$ and $(Mg_{0.75}Fe_{0.25})O$ samples contained ~2% and 7% of the ferric Fe^{3+} iron $[Fe^{3+}/(Fe^{2+}+Fe^{3+})]$, respectively (14). The small amount of ferric Fe^{3+} ions may be localized either in interstitial sites or in substitution for the octahedral Mg sites, forming dimers with cation vacancies (□) to balance the molecular electroneutrality (51) $(Fe^{3+} - □ - Fe^{3+}) = 3Fe^{2+}$.

At ambient pressure, the ^{57}Fe-Mössbauer spectra were recorded in the temperature range of 4.2–300 K in the transmission geometry with a standard spectrometer operating in the constant accelerations regime (the TMS technique). The gamma-ray source $^{57}Co(Rh)$ was used at room temperature, and the isomer shifts were measured relative to α-Fe metal at room temperature. Average values of the magnetic hyperfine field $\langle H_{hf} \rangle$ at iron nuclei were estimated from the distribution functions of the hyperfine parameters constructed for widened spectral lines (25).

High-pressure synchrotron Mössbauer spectroscopic technique (NFS) was applied to study magnetic and electronic spin states of iron ions in $(Mg_{0.75}Fe_{0.25})O$ at pressures of up to 60 GPa and temperatures ranging from 8 K to 300 K. For the NFS measurements, powder $(Mg_{0.75}Fe_{0.25})O$ samples were flattened down to ~3-μm–thick disks between two diamond anvils. Rhenium gaskets were preindented to a thickness of 25 μm, and a hole of 80 μm was drilled in them. Small disks of the samples with a size ~50 × 50 μm^2 were loaded into the sample chambers of the DACs with flat diamonds of 300 μm in culet size. The low-temperature NFS experiments were carried out in quasi-hydrostatic conditions with silicon oil (poly-ethyl-siloxane 5) as a pressure medium. The synchrotron beam size was focused to a small spot of about 7 × 7 μm^2, which allowed us to collect all NFS spectra over an extremely small sample area that provided nearly hydrostatic conditions with negligible pressure gradients. Several ruby chips, each 1–2 μm in diameter, were placed next to the samples in the chambers for in situ pressure determinations and evaluations of the pressure gradients, which showed that the pressure gradients of the measured sample areas did not exceed 2 GPa at the maximum experimental pressure of 60 GPa.

A specially designed DAC (52) and small cryostat have been used for the low-temperature measurements, in which pressure can be held stable during the cooling process to 4.2 K. Temperatures of the sample chambers were controlled within ±2 K using a feedback power supply unit. We also carefully measured the high-pressure TMS and NFS spectra at room temperature. The TMS spectra were recorded at pressures up to 78 GPa and NFS spectra at pressures up to 92 GPa, both in hydrostatic conditions with helium as the pressure medium. The room-temperature data are discussed in *SI Materials and Methods*. The NFS measurements in DAC were carried out at the beamline 16-IDD of the Advanced Photon Source, Argonne National Laboratory (7). The measured NFS spectra were analyzed with the Motif program (30).

ACKNOWLEDGMENTS. We thank Yu. S. Orlov and A. Wheat for useful discussion. This work is supported by Russian Foundation for Basic Research Grants 11-02-00636, 10-02-00251, 11-02-00291, 12-02-90410, and 12-02-31543; Siberian Branch of Russian Academy of Science Integration Grant 96; Grant NSh-1044.2012.2; Siberian Federal University Grant F11; Presidium Russian Academy of Science (RAS) Program 2.16; and RAS Program "Elementary partical physics, fundamental nuclear physics, and nuclear technologies." Support from US Department of Energy (DOE) Grant DE-FG02-02ER45955 for the work at Carnegie and at the Advanced Photon Source (APS) synchrotron facility is greatly acknowledged. The work at University of Texas at Austin was supported by the US National Science Foundation [(NSF) EAR-0838221], the Energy Frontier Research in Extreme Environments Center, and the Carnegie/DOE Alliance Center. The synchrotron Mössbauer work was performed at HPCAT (Sector 16), APS, Argonne National Laboratory. High Pressure Collaborative Access Team is supported by DOE-BES, DOE-National Nuclear Security Administration, NSF (EAR-1119504), and the W. M. Keck Foundation. APS is supported by DOE-BES under Contract DE-AC02-06CH11357.

1. Pushcharovskii DY (2002) Minerals of the deep geospheres. *Phys Usp* 45(4):439–444.
2. Jeanloz R, Knittle E (1989) Density and composition of the lower mantle. *Philos Trans R Soc London Ser A* 328(1599):377–389.
3. Shearman DM (1991) The high-pressure electronic structure of magnesiowustite (Mg,Fe)O: Applications to the physics and chemistry of the lower mantle. *J Geophys Res* 96(B9):14299–14312.
4. Pushcharovskii DY (1980) The earth's deep minerals. *Rus J Nature (Priroda)* 11: 119–120.
5. Lee KKM, et al. (2004) Equations of state of the high-pressure phases of a natural peridotite and implications for the earth's lower mantle. *Earth Planet Sci Lett* 223(3–4):381–393.
6. Chalabov RI, Lyubutin IS, Zhmurova ZI, Dodokin AP, Dmitrieva TV (1982) Mossbauer study of the non-stoichiometry defects in wustite crystals. *Sov Phys Crystallogr* 27(3): 312–315.
7. Lin JF, et al. (2006) Pressure-induced electronic spin transition of iron in magnesiowustite-(Mg,Fe)O. *Phys Rev B* 73(11):113107.
8. Kantor IY, Dubrovinsky LS, McCommon CA (2006) Spin crossover in (Mg,Fe)O: A Mossbauer effect study with an alternative interpretation of x-ray emission spectroscopy. *Phys Rev B* 73(10):100101.
9. Gavriliuk AG, Lin JF, Lyubutin IS, Struzhkin VV (2006) Optimization of the conditions of synchrotron Mossbauer experiment for studying electronic transitions at high pressure by the example of (Mg, Fe)O magnesiowustite. *JETP Lett* 84(3):161–166.
10. Lin JF, Struzhkin VV, Gavriliuk AG, Lyubutin IS (2007) Comment on "Spin crossover in (Mg,Fe)O: A Mossbauer effect study with an alternative interpretation of x-ray emission spectroscopy data. *Phys Rev B* 75(17):177102.
11. Li J (2007) *Post-Perovskite: The Last Mantle Phase Transition*, eds Hirose JBK, Lay T, Yuen D (American Geophysical Union, Washington, DC).
12. Lin JF, Jacobsen SD, Wentzcovitch RM (2007) Electronic spin transition of iron in the earth's deep mantle. *Eos* 88:13–24.
13. Lin JF, et al. (2009) Synchrotron Mössbauer spectroscopic study of ferropericlase at high pressures and temperatures. *Am Mineral* 94(4):594–599.
14. Lyubutin IS, Gavriliuk AG, Frolov KF, Lin JF, Trojan IA (2009) High-spin low-spin transition in $Mg_{0.75}Fe_{0.25}O$ magnesiowustite at high pressures under hydrostatic conditions. *JETP Lett* 90(9):617–622.
15. Goncharov AF, Struzhkin VV, Jacobsen SD (2006) Reduced radiative conductivity of low-spin (Mg,Fe)O in the lower mantle. *Science* 312(5777):1205–1208.
16. Keppler H, Kantor IY, Dubrovinsky LS (2007) Optical absorption of spectra ferropericlase to 84 GPa. *Am Mineral* 92(2–3):433–436.
17. Lin JF, Weir ST, Jackson DD, Evans WJ, Yoo CS (2007) Electrical conductivity of the lower-mantle ferropericlase across the electronic spin transition. *Geophys Res Lett* 34(16):L16305.
18. Lin JF, et al. (2005) Spin transition of iron in magnesiowüstite in the earth's lower mantle. *Nature* 436(7049):377–380.
19. Fei Y, et al. (2007) Spin transition and equation of state of (Mg,Fe)O solid solutions. *Geophys Res Lett* 34(17):17307.
20. Lin JF, et al. (2005) Sound velocities of hot dense iron: Birch's law revisited. *Science* 308(5730):1892–1894.
21. Speziale S, et al. (2005) Iron spin transition in Earth's mantle. *Proc Natl Acad Sci USA* 102(50):17918–17922.
22. Ovchinnikov SG (2003) Many-electron model of band structure and metal-insulator transition under pressure in $FeBO_3$. *JETP Lett* 77(12):676–679.
23. Ovchinnikov SG (2005) The mechanism of the electronic transition in ferroborates under high pressure. *J Phys Condens Matter* 17(11):S743–S751.
24. Wertheim GK ed (1964) *Mossbauer Effect. Principles and Applications* (Academic, New York).
25. Rusakov VS (2000) *Mössbauer Spectroscopy of Locally Heterogeneous Systems* [*Messbauerovskaya Spektroskopiya Lokal'no Neodnorodnykh Sistem*]. (Nuclear Physics Institute, Almaty, Kazakhstan). Russian.
26. Roth WL (1960) Defects in the crystal and magnetic structures of ferrous oxides. *Acta Crystallogr* 13(2):140–149.
27. Ziman JM (1979) *Models of Disorder* (Cambridge Univ Press, Cambridge, UK).
28. Cotton E (1960) Emission and absorption of gamma-rays without recoil of the emitting nucleus, held in a crystal lattice (Mossbauer effect). *J Phys Radium* 21(5):265–287.
29. Smirnov GV (1999) General properties of nuclear resonant scattering. *Hyperfine Interact* 123-124(1–4):31–77.
30. Shyd'ko YV (1999) Nuclear resonant forward scattering of x-rays: Time and space picture. *Phys Rev B* 59(14):9132–9143.
31. Sachdev S (2001) *Quantum Phase Transition* (Cambridge Univ Press, Cambridge, UK).
32. Nesterov AI, Ovchinnikov SG (2009) Spin crossover: The quantum phase transition induced by high pressure. *JETP Lett* 90(7):530–534.
33. Lyubutin IS, et al. (2006) Pressure-induced electron spin transition in the paramagnetic phase of the $GdFe_3(BO_3)_4$ Heisenberg magnet. *JETP Lett* 84(9):518–523.
34. Lyubutin IS, Gavriliuk AG (2009) Research on phase transformations in 3d-metal oxides at high and ultrahigh pressure: State of the art. *Phys. Usp* 52(10):989–1017.
35. Gavriliuk AG, et al. (2008) Another mechanism for the insulator-metal transition observed in Mott insulators. *Phys Rev B* 77(15):155112.
36. Lin JF, et al. (2007) Spin transition zone in Earth's lower mantle. *Science* 317(5845): 1740–1743.
37. Gavriliuk AG, Trojan IA, Ovchinnikov SG, Lyubutin IS, Sarkisyan VA (2004) The mechanism of suppression of strong electron correlations in $FeBO_3$ at high pressures. *Sov Phys JETP* 99(3):566–573.
38. Tanabe Y, Sugano S (1954) On the absorption spectra of complex ions II. *J Phys Soc Jpn* 9:766–779.
39. Ropka Z, Radwanski RJ (2003) 5D term origin of the excited triplet in $LaCoO_3$. *Phys Rev B* 67(17):172401.
40. Haverkort MW, et al. (2006) Spin state transition in $LaCoO_3$ studied using soft x-ray absorption spectroscopy and magnetic circular dichroism. *Phys Rev Lett* 97(17): 176405.
41. Ovchinnikov SG, Orlov YS, Nekrasov IA, Pchelkina ZV (2011) Electronic structure, magnetic properties, and mechanism of the insulator-metal transition in $LaCoO_3$ taking into account strong electron correlations. *Sov Phys JETP* 112(1):140–151.
42. Sturhahn W, Jackson JM, Lin JF (2005) The spin state of iron in mineral of Earth's lower mantle. *Geophys Res Lett* 32:L12307.
43. Tsuchiya T, Wentzcovitch RM, da Silva CRS, de Gironcoli S (2006) Spin transition in magnesiowüstite in earth's lower mantle. *Phys Rev Lett* 96(19):198501.
44. Wu Z, et al. (2009) Anomalous thermodynamical properties of ferropericlase throughout its spin crossover transition. *Phys Rev B* 80(1):014409.
45. Wentzcovitch RM, et al. (2009) Anomalous compressibility of ferropericlase throughout the iron spin cross-over. *Proc Natl Acad Sci USA* 106(21):8447–8452.
46. Hsu H, Umemoto K, Wu Z, Wentzcovitch RM (2010) Spin-state crossover of iron in lower-mantle mineral: Results of DFT+U investigations. *Rev Mineral Geochem* 71: 169–199.
47. Xu Y, Shankland TJ, Poe BT (2000) Laboratory-based electrical conductivity in the earth's mantle. *J Geophys Res* 105(B12):27865.
48. Zerr A, Boehler R (1994) Constraints on the melting temperature of the lower mantle from high-pressure experiments on MgO and magnesiowustite. *Nature* 371:506–508.
49. Vocadlo L, Price GD (1996) The melting of MgO—Computer calculations via molecular dynamics. *Phys Chem Miner* 23:42–49.
50. Cohen RE, Gong Z (1994) Melting and melt structure of MgO at high pressures. *Phys Rev B* 50(17):12301–12311.
51. Dobson DP, Cohen NS, Pankhurst QA, Brotholt JP (1998) A convenient method for measuring ferric iron magnesiowustite ($MgO\text{-}Fe_{1-x}O$). *Am Mineral* 83(7–8):794–798.
52. Gavriliuk AG, Mironovich AA, Struzhkin VV (2009) Miniature diamond anvil cell for broad range of high pressure measurements. *Rev Sci Instrum* 80(4):043906.